Article

Research on Frequency Response Modeling and Frequency Modulation Parameters of the Power System Highly Penetrated by Wind Power

Junfeng Qi, Fei Tang *, Jiarui Xie, Xinang Li, Xiaoqing Wei and Zhuo Liu

School of Electrical Engineering and Automation, Wuhan University, Wuhan 430072, China;
qijunfeng@whu.edu.cn (J.Q.); xiejiarui@whu.edu.cn (J.X.); 2017302540172@whu.edu.cn (X.L.);
weixiaoqing@whu.edu.cn (X.W.); 2018302070205@whu.edu.cn (Z.L.)
* Correspondence: tangfei@whu.edu.cn

Abstract: Renewable energy units led by wind power participate in diversified control primary frequency modulation, making the frequency response modes and the setting of frequency modulation parameters more complex. This paper proposes a frequency response model of the power system which is highly penetrated by wind power based on the two mainstream control strategies of wind power that participate in primary frequency modulation. The model considers the influence of wind capture devices, maximum power point tracking (MPPT), and other complex control strategies on system frequency response. Based on this model, the calculation formulas of the maximum change rate of dynamic frequency, the lowest point of dynamic frequency, and the maximum steady-state frequency deviation of the system after fault disturbance are derived in the frequency domain. The influences of wind power permeability and two typical frequency response control strategies on system frequency stability are analyzed. On the one hand, it is found that the proposed model can fit the system frequency response better than the traditional system frequency response model. Beyond that, two control strategies are mainly aimed at the different frequency stability requirements. On the other hand, under the condition of meeting the system's stability requirements, the paper calculates the control parameters of frequency response of the doubly-fed induction generator (DFIG). The time-domain simulation model of the improved IEEE three-machine nine-node system and IEEE 39-node system with high permeability of wind power are built. Through the different fault scenarios, the simulation results verify the effectiveness of the proposed model and the accuracy of control strategy parameter calculation.

Keywords: frequency response model; highly penetrated by wind power; virtual droop control; virtual inertia control

1. Introduction

1.1. Background and Literature Review

1.1.1. Background

The world's energy problems are significant, and renewable energy units will play a leading role in the power supply of the power system [1,2]. The renewable energy high penetration power system represented by wind power is gradually formed, and the wind power control strategy is much more complex. The traditional system frequency response model (TSFR) cannot fit the existing frequency response of the system [3,4]. The doubly-fed induction generator (DFIG) is one of the most mature wind turbine generators. It is important to study the participation of new energy units represented by DFIG in frequency response [5]. According to the requirements of system frequency stability, it is of great practical engineering significance to analyze the impact of the DFIG control strategies on system frequency response. Meanwhile, it is necessary to evaluate the frequency stability of the system quantitatively.

1.1.2. The Impact of Strategies of DFIG on Frequency Response

When large-scale wind turbines are connected to the power grid through a power electronic converter, the equivalent inertia of the system is reduced, and the ability of the system to resist frequency disturbance is reduced [4–6]. With the improvement of the power system's wind power penetration, developed countries in Europe and North America have required that the wind turbine should have inertia response and primary frequency regulation capability. At present, the frequency response of wind power is relatively mature, and the control strategies mainly include virtual inertia control, virtual droop control, and over-speed load shedding [7–9]. Reference [10] analyzes the impact of the two kinds of control strategies on frequency response. It finds that the two control strategies can enhance power system stability by improving the system's inertia, but it does not consider the DFIG's operating state. References [11–13] find that fast frequency support from DFIG can provide inertial response considering the rotor security. References [14–17] introduce the virtual inertia control strategy and virtual droop control strategy in the control of rotor side converter and omit the phase-locked loop link. They verify that the virtual inertial control has good stable supportability for the system's inertia, and the virtual droop control can enhance the primary frequency response.

1.1.3. The Research on System Frequency Response Model

It simplifies the analysis of system frequency response based on the low order TSFR. The key to frequency analysis is to build the SFR fitting the actual system and determine the analysis indexes. Fangxing Li et al. propose the calculation method of system equivalent parameters and verify its effectiveness in [18].

Hanyu Li et al. take the specific control strategy of DFIG into account in the SFR model in [19], which is conducive to further analyzing the frequency response characteristic. Ziping Wu et al. elaborate various control strategies for frequency regulation by wind power, and a variety of SFR models considering the different strategies in [20]. And they prospect the methods and strategies to improve the frequency dynamic response.

The commonly used indexes to measure the frequency stability ability of a power system include the maximum rate of change of system frequency ($RoCoF_{max}$), the lowest point of system dynamic frequency, and the maximum deviation of system steady-state frequency [21,22].

Based on the simplified TSFR, reference [22] proposes a simplified frequency model for the system highly penetrated by renewable power. Moreover, based on this model, reference [22] qualitatively analyzes the impact of new energy permeability and new energy primary frequency modulation response strategy on system frequency stability. However, the model does not consider the specific new energy control strategy, so the fitting degree with the frequency response of the actual system is low. Reference [23] analyzes the impact of wind power participation in primary frequency modulation on the system frequency response and analyzes the influencing factors. However, it does not take further strategies into account in the system equivalent model, such as wind energy capture devices and maximum power point tracking (MPPT). Considering the inertia proportion coefficient, references [8,24] propose the frequency analysis model of new energy highly penetrated system, which can reflect the overall inertia and primary frequency regulation characteristics of the system. This model can fit the actual frequency response well but does not conduct quantitative calculation and analysis for specific frequency response control parameters. References [25,26] analyze that wind power participation in frequency modulation can effectively improve the limit value of wind power proportion under frequency constraints. References [18–26] have studied that the participation of wind power in system frequency modulation will affect the fitting degree of SFR to the system. They also find that different control strategies aim at various frequency stability problems of the system and have different effects on the dynamic and steady-state frequency responses. This makes the system frequency more complicated and the control parameters more challenging to set.

1.2. Research Gap and Motivation

In conclusion, research on the frequency response of wind power participation has matured. There is an increasing amount of research on SFR modeling that considers the complex control strategies of new energy units. However, there is too little research on quantitative calculation of system stability index and SFR considering the complex strategies of wind power.

Most of the research only conducts qualitative analysis on the influence of wind power permeability on system frequency. Few researches calculate the DFIG's frequency modulation parameters that meet the system's requirements according to the frequency response formula. Improving the existing SFR model and deriving the system frequency response formula in combination with the system frequency stability requirements is of great engineering significance.

1.3. Contribution and Organization

1.3.1. Contribution of This Paper

Based on the shortcomings of existing research, the main contributions of this paper are as follows:

- The frequency response model of the wind power highly penetrated system proposed this paper can fit the actual system better than TSFR.
- The calculation formulas of three indexes of system frequency stability are derived based on this model.
- The different effects of virtual inertia and virtual droop control strategies on the frequency response of the system are analyzed.
- The parameter setting of DFIG participating in frequency modulation is calculated according to the frequency stability requirements of the actual system.

1.3.2. Organization of This Paper

The paper is organized as follows:

Section 2 proposes the improved frequency response model of the wind power highly penetrated system based on the existing researches. Section 3 derives the calculation formulas of three indexes of system frequency response stability and analyzes the impact of the virtual inertia and virtual droop control on the different indexes. Section 4 verifies the validity of the proposed frequency response model and the accuracy of parameter calculation. In Section 5, the paper draws a conclusion and shows the research prospects.

2. Frequency Response Model of the Wind Power Highly Penetrated System

2.1. Frequency Response Model of Traditional Power System

The frequency of the power system is always in the process of dynamic adjustment. According to different time scales, the traditional generator sets will adjust the system's frequency by inertia response, primary frequency regulation, and secondary frequency regulation to ensure the stable operation of the system. The traditional frequency response (TSFR) model of the power system is shown in Figure 1, and it can be obtained that the frequency response process of the system is a closed-loop process [27]. The frequency response capability of a traditional power system mainly depends on the parameters of the synchronous generator set and the load response capability of the system.
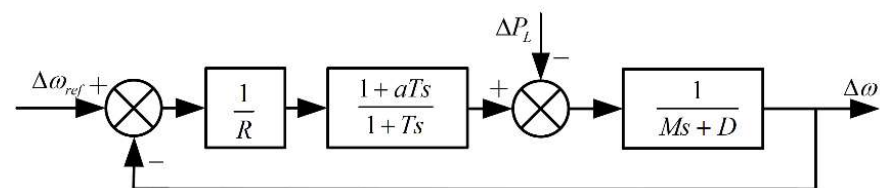
Figure 1. The traditional frequency response model of the power system.

In Figure 1, ΔP_L is the disturbance power, Δw and Δw_{ref} are system frequency deviation and reference value, respectively; a is the turbine coefficient of the turbine generator; T is the equivalent time constant of the turbine; M is the rotor time constant; $1/R$ is governor gain; D is the frequency response coefficient of the load. The multi-machine system parameters can be equivalent to the single machine system parameters according to [18].

Define the speed regulation function $G_1(s)$ of the power system and the frequency response function $G_2(s)$ of the engine load:

$$\begin{cases} G_1(s) = \frac{1}{R} \frac{1 + aTs}{1 + Ts} \\ G_2(s) = \frac{1}{Ms + D} \end{cases} \tag{1}$$

According to Equation (1), the frequency domain expression of traditional power system frequency can be deduced:

$$\Delta w = \frac{w_{ref} G_1(s) G_2(s) - \Delta P_L G_2(s)}{1 + G_1(s) G_2(s)} \tag{2}$$

With the formation of a power system with high penetration of new energy, the frequency modulation ability of new energy units will determine the frequency response-ability of the system. Therefore, the TSFR model shown in Figure 1 cannot fit the frequency response characteristics of the existing procedure.

2.2. Wind Power System Modeling

The frequency modulation capability of wind turbines mainly depends on the unit capacity and control strategy involved in frequency modulation [28]. The complete control strategy of wind turbines specifically includes wind energy capture control, MPPT control, converter control, and frequency response control.

Wind energy utilization coefficient $C_p(\lambda, \beta)$ determines the efficiency of wind energy captured by turbines [13]. Affected by the control mode and ambient wind speed, $C_p(\lambda, \beta)$ is in dynamic change:

$$\begin{cases} P_m = \frac{1}{2} \rho V^3 S C_p(\lambda, \beta) \\ C_P = 0.22 \left(\frac{116}{\lambda_i} - 0.4\beta - 5 \right) e^{-12.5/\lambda_i} \\ \frac{1}{\lambda_i} = \frac{1}{\lambda + 0.08\beta} - \frac{0.035}{\beta^3 + 1} \\ \lambda = \frac{\omega_r R}{V} \end{cases} \tag{3}$$

where P_m is the power captured by wind turbines; ρ is the air density; V is the upwind speed of the wind turbine rotor; S is the area of wind turbine blades; λ is the tip speed ratio; β is the pitch angle.

When the β is constant, in order to calculate the change of input ΔP_m caused by the change of wind speed ΔV and rotor frequency Δw_r, the function fitting method can be used to reduce the amount of calculation:

$$P_m = m_1 w_r^3 + m_2 w_r^2 v + m_3 w_r v^2 + m_4 v^3 \tag{4}$$

The corresponding mechanical power change ΔP_m due to the evolution of rotor frequency Δw and wind speed ΔV is as follows:

$$\Delta P_m = \frac{\partial P_m}{\partial w_r} \Delta w_r + \frac{\partial P_m}{\partial v} \Delta v \tag{5}$$

The rotor inner loop current controls the output power P_e, and the rotor outer loop control is diverse. The multi-loop control strategy leads to the decoupling of the rotor

frequency and grid frequency. However, the variation of DFIG input and output power is provided by the interpretation of rotor kinetic energy:

$$\Delta E_k = \frac{1}{2} J_{DFIG} \left(w_r^2 - (w_r + \Delta w_r)^2 \right) \tag{6}$$

where the J_{DFIG} is the rotor inertia of DFIG.

Defined by the rotor inertia time constant:

$$\frac{\Delta E_k}{S_B} = 2 H_{eq} \frac{dw_r}{dt} \tag{7}$$

When the sampling time is the unit time dt, and the unit frequency change Δw_r occurs, the calculation method of the DFIG inertia time constant can be obtained:

$$H_{eq} = \frac{J_{DFIG} \left(w_r^2 - (w_r + \Delta w_r)^2 \right)}{4 \Delta w_r} \tag{8}$$

MPPT control realizes maximum power tracking through control Δw_r, so the change of DFIG root speed will affect ΔP_{MPPT}:

$$\Delta P_m = k_{opt} \Delta w_r{}^3 \tag{9}$$

where the k_{opt} is the maximum power tracking coefficient of MPPT.

The DFIG involved in the frequency response control of the system analyzed in this paper is virtual droop and virtual inertia control [16].

$$\begin{cases} \Delta P_{df} = A_1 \cdot \Delta w \\ \Delta P_{if} = A_2 \cdot \frac{d \Delta w}{dt} \end{cases} \tag{10}$$

where A_1 is the gain of virtual droop control and A_2 is the gain of virtual inertia control.

Assuming that all DFIG units in the system participate in the frequency response of the system, the wind power permeability K is defined as follows:

$$K = \frac{\text{Installed capacity of wind power (MW)}}{\text{system load power (MW)}} \tag{11}$$

Combined with the traditional simplified model of power system frequency and according to formulas (3), (8), (9), (10), and (11), the frequency response model of the wind power highly penetrated system can be obtained as follows:

As shown in Figure 2, the improved SFR model consists of frequency response model of DFIG and the traditional frequency response model. The model is proposed after improvement based on the models in [19,20,22,28]. P_{wind} can reflects the change of system frequency by the virtual control strategies and wind speed by the MPPT strategy. The wind power permeability is adjusted through K. The calculation of system parameters is the same as that of TSFR [18], and the whole wind farm is equivalent to a DFIG.

The TSFR model in [27] provides a theoretical basis for the analysis of the frequency response of the power system. The model in [20] considers various frequency response strategies of wind power. This paper draws on two mature virtual response control strategies. The SFR model proposed combines the advantages of models in [19,20,22]. Compared with the models in [19,22], the model considers not only the permeability of wind power, but also the complex and specific strategies of DFIG. Compared with the model in [20], the model can reflect not only the permeability of the wind power but also the effect about rotor frequency Δw_r to the system frequency. Therefore, it can fit the actual power system better than the TSFR.
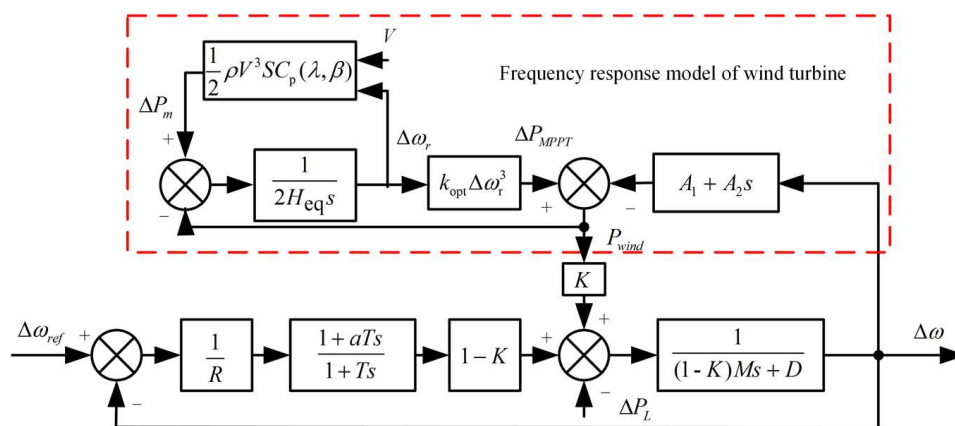
Figure 2. The frequency response model of the wind power highly penetrated system.

2.3. Model Frequency Response Analysis

When ΔP_{MPPT} due to Δw_r and ΔV is ignored, the equivalent powertrain speed regulation function $G_1{}'(s)$ and the equivalent engine load frequency response function $G_2{}'(s)$ are defined according to Figure 2 as follows:

$$\begin{cases} G_1{}'(s) = \dfrac{1-K}{R}\dfrac{1+aTs}{1+Ts} \\ G_2{}'(s) = \dfrac{1}{[(1-K)M+KA_2]s+D+KA_1} \end{cases} \tag{12}$$

For the convenience of calculation, the equivalent turbine response coefficient, rotor time constant, and equivalent load dynamic response coefficient can be defined as follows:

$$\begin{cases} \dfrac{1}{R'} = \dfrac{1-K}{R} \\ M' = (1-K)M+KA_2 \\ D' = D+KA_1 \end{cases} \tag{13}$$

Therefore, the simplified equivalent response function can be obtained as follows:

$$\begin{cases} G_1{}'(s) = \dfrac{1}{R'}\dfrac{1+aTs}{1+Ts} \\ G_2{}'(s) = \dfrac{1}{M's+D'} \end{cases} \tag{14}$$

Comparing Formulas (1) and (14), the increase of new energy permeability will reduce the frequency response-ability of the system equivalent power system and unit rotor, reducing the system's equivalent inertia. In fact, the participation of new energy in frequency modulation improves the reduction of system equivalent inertia and increases the load frequency response-ability.

According to Formula (14), the frequency domain expression of frequency can be obtained as follows:

$$\Delta w(s) = \frac{\Delta w_{ref} G_1{}'(s)G_2{}'(s) - \Delta P_L G_2{}'(s)}{1+G_1{}'(s)G_2{}'(s)} \tag{15}$$

The system has equal proportional power disturbance at 10 s, and the frequency change can be obtained according to Formula (15), as shown in Figure 3.
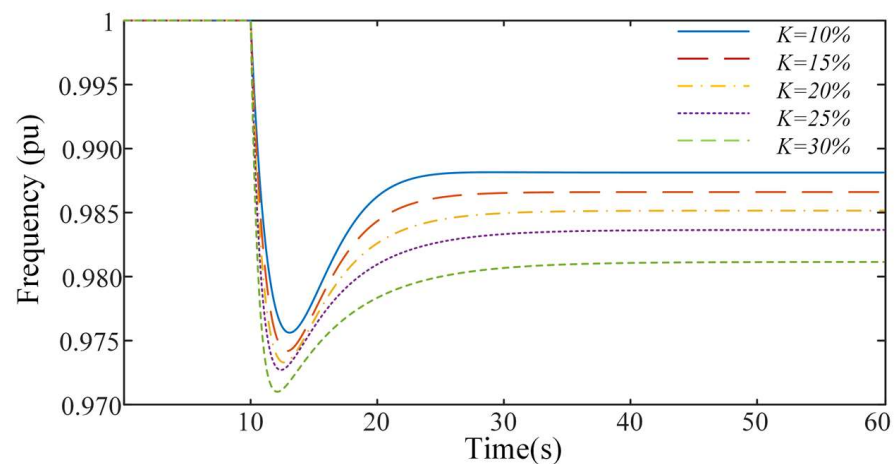
Figure 3. System frequency response under different wind power permeability.

Under the same frequency response control coefficient, the system frequency response curve is obtained by changing the permeability of wind power. It can be obviously observed that with the increase of the wind power permeability, the lowest point of the system dynamic frequency and the steady-state frequency will decrease, which also verifies that the increase of the new energy permeability will reduce the system's equivalent inertia.

By setting the same wind power permeability and different frequency response control parameters, the frequency response curve is shown in Figure 4. Under the same wind power permeability, the maximum change rate of dynamic frequency (RoCoF$_{max}$), the lowest point of dynamic frequency and the maximum deviation of steady-state frequency can be effectively improved by reasonably setting the frequency response parameters of wind power. Thus, the frequency deterioration caused by the increase of wind power permeability can be improved. At the same time, it shows that the virtual inertial control can effectively improve the frequency change rate, and the virtual droop control can effectively improve the dynamic frequency lowest point and steady-state frequency deviation of the system.
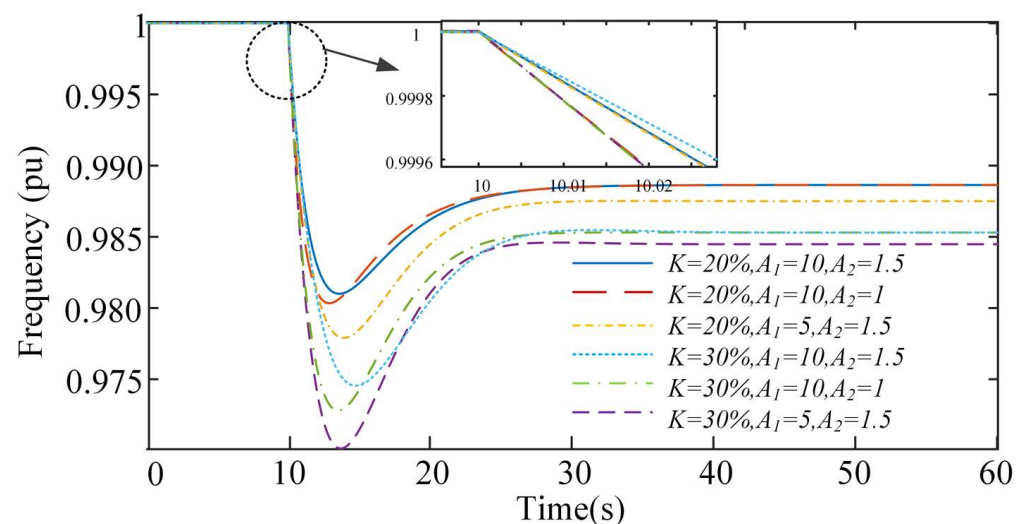
Figure 4. Influence of different control parameters on system frequency.

3. Frequency Stability Analysis of the Wind Power Highly Penetrated System

In case of power or frequency disturbance in the power system, the system frequency shall be fed back to each primary frequency modulation equipment in time. The system frequency shall be maintained stable after closed-loop processing. According to the improved

SFR model shown in Figure 2, the relationship between the frequency stability of the wind power high permeability power system and various control parameters can be analyzed in the frequency domain.

3.1. Steady-State Performance Analysis of Closed-Loop System

The model proposed in this paper is a typical closed-loop system so that control engineering can be used for stability analysis. Combined with Figure 2 and Formulas (12)–(14), the closed-loop transfer function of the system can be obtained as follows:

$$H(s) = \frac{G_1'(s)G_2'(s)}{1 + G_1'(s)G_2'(s)} = \frac{a'}{R'M'} \cdot \frac{s + \frac{1}{a'T}}{s^2 + \frac{R'M' + R'TD' + a'T}{R'M'T}s + \frac{R'D' + 1}{R'M'T}} \tag{16}$$

Therefore, the characteristic equation parameters of the closed-loop system can be obtained as follows:

$$\begin{cases} w_n^2 = \frac{R'D' + 1}{R'M'T} \\ 2\zeta w_n = 2 \cdot \frac{R'M' + R'D'T + 2a'T}{R'M'T} \end{cases} \tag{17}$$

Without considering hydropower, that is, when $a > 0$, the following can be obtained:

$$\begin{cases} w_n^2 = \frac{1}{T} \cdot \frac{R(D + KA_1) + 1 - K}{RM(1 - K) + KA_2} > 0 \\ 2\zeta w_n = 2 \left(\frac{1}{T} + \frac{D + KA_1}{(1 - K)M + KA_2} + \frac{2}{R} \frac{a(1 - K)}{(1 - K)M + KA_2} \right) > 0 \end{cases} \tag{18}$$

According to the above analysis, when the external disturbance is not considered, the wind power permeability K and various control parameters will not affect the stable closed-loop of the system frequency. Therefore, the research focus should be on quickly restoring the system's stable parameter setting of the system when the system is disturbed.

3.2. Analysis of the Maximum Rate of Change of Frequency of System Dynamic Frequency

The rate of change of frequency (RoCoF) of the power system is too large, which easily causes the action of the relay protection device. It is an important index to measure the ability of the system to resist disturbance. The $\text{RoCoF}_{\max}$ of the system occurs at the initial stage of the fault. At this time, the system frequency deviation Δw is slight and approaches 0.

The frequency error transfer function $\Delta w(s)$ based on power disturbance in Figure 2 is defined as follows:

$$\Delta w(s) = \frac{G_2'(s)}{1 + G_1'(s)G_2'(s)} \Delta P_L \tag{19}$$

The $\text{RoCoF}_{\max}$ of the dynamic frequency response of the system can be obtained by the Laplace initial value theorem transformation calculation of formula (19):

$$RoCoF_{\max} = \lim_{t \to 0} \frac{dw(t)}{dt} = \lim_{s \to \infty} s \cdot s \cdot \frac{1}{s} (\Delta w(s)) = \frac{\Delta P_L}{M'} \tag{20}$$

where the M' is the variable of permeability and virtual inertia control parameters.

The smaller $\text{RoCoF}_{\max}$ is, the stronger the system resistance to disturbance is. With the increasing permeability of the wind power, $\text{RoCoF}_{\max}$ will depend on the size of the virtual inertia control parameter A_2.

Therefore, when determining the wind power permeability K and the threshold η_1 of system transient time-domain frequency change rate, the value of virtual inertia control parameter A_2 can be defined as follows:

$$A_2 > \Delta P_L \left(\frac{1}{|\eta_1| K} - \frac{(1 - K)M}{K} \right) \tag{21}$$

3.3. Analysis of Lowest Point of System Dynamic Frequency

This section uses the closed-loop transfer function of power disturbance to analyze the influence of different wind power frequency response control parameters on the lowest point of system dynamic frequency when step power disturbance occurs.

According to the frequency error transfer function (19), the closed-loop transfer function of the system can be obtained as follows:

$$E(s) = \frac{\Delta w(s)}{-\Delta P_L} = -\frac{G_2'(s)}{1 + G_1'(s)G_2'(s)} = -\left\{ \frac{R'}{1 + R'D'} \frac{B}{s^2 + As + B} + \frac{1}{M'(Y-X)} \left(\frac{Y}{s+Y} - \frac{X}{s+X} \right) \right\} \tag{22}$$

Define new variables to simplify the calculation, where:

$$\begin{cases} A = \frac{1}{T} + \frac{D'}{M'} + \frac{a}{R'M'} \\ B = \frac{1+R'D'}{R'TM'} \end{cases}$$

$$\begin{cases} 2w_n\xi = A \\ w_n^2 = B \end{cases} \tag{23}$$

$$\begin{cases} X + Y = A \\ XY = B \end{cases}$$

Therefore, when the step power disturbance occurs in the system, the system frequency response function in the time domain can be written:

$$h(t) = -\left\{ \frac{R'}{1 + R'D'} \left[1 - \frac{1}{\sqrt{1-\xi^2}} e^{-\xi w_n t} \sin(\sqrt{1-\xi^2} w_n t + \cos^{-1}\xi) \right] + \frac{1}{M'(Y-X)} (Xe^{-Xt} - Ye^{-Yt}) \right\} \tag{24}$$

Derive formula (22) and calculate the peak value. At the same time $\xi < 1$ (underdamped state), the time of the occurrence is as follows:

$$t_p = \frac{\arctan(\frac{\sqrt{1-\xi^2}}{\xi}) + \arctan(\frac{\sqrt{1-\xi^2}}{\frac{w_n}{T}-\xi})}{\sqrt{1-\xi^2} w_n} \tag{25}$$

The lowest point of dynamic frequency in the time domain is as follows:

$$h(t_p) = 1 - \sqrt{1 - \frac{2\xi w_n}{T} + (\frac{w_n}{T})^2} \exp(-\xi w_n t_p) \tag{26}$$

Both ξ and w_n is related to A_1 and A_2. The relationship between A_1 and A_2 can be determined by determining the maximum frequency deviation threshold η_2 in the transient time domain of the system.

$$\eta_2 > \sqrt{1 - \frac{2\xi w_n}{T} + (\frac{w_n}{T})^2} \exp(-\xi w_n t_p) \tag{27}$$

3.4. Analysis of Steady-State Frequency Deviation of the System

System steady-state frequency is an important parameter to characterize the long-term power quality of the system. In this section, the error transfer function of power disturbance is used to analyze the influence of A_1 and A_2 parameter settings on the system's frequency response in case of a power disturbance.

According to Laplace's final value theorem and formula (19), the maximum deviation of system steady-state frequency can be obtained as follows:

$$\Delta w_\infty = \lim_{t \to \infty} \Delta w(t) = \lim_{s \to 0^+} s\Delta w(s) = \frac{\Delta P_L}{D + KA_1 + \frac{1-K}{R}} \tag{28}$$

When the power disturbance occurs in the system, the smaller the maximum deviation of the steady-state frequency of the system, the more stable the system is. When the wind power permeability of the system is higher and higher, the steady-state frequency capability of the system mainly depends on the virtual droop control of the fan. Virtual inertial control does not affect the steady-state frequency deviation of the system.

Therefore, when the maximum allowable deviation threshold η_3 and the wind power permeability K of the system are determined, the size of the virtual droop control parameter A_1 can be determined.

$$A_1 > \frac{\Delta P_L}{\eta_3 K} - \frac{1-K}{RK} - \frac{D}{K} \tag{29}$$

4. Case Study

4.1. Simulation Model Construction

4.1.1. Small-Scale System

The IEEE three-machine nine-node simulation system with a high proportion wind power grid connection is built by using the MATLAB/Simulink platform. Based on this, this section will verify the effectiveness of the proposed frequency response model of wind power highly penetrated the system and the accuracy of parameter calculation of two frequency response control strategies of the DFIG. The system structure topology is shown in Figure 5.
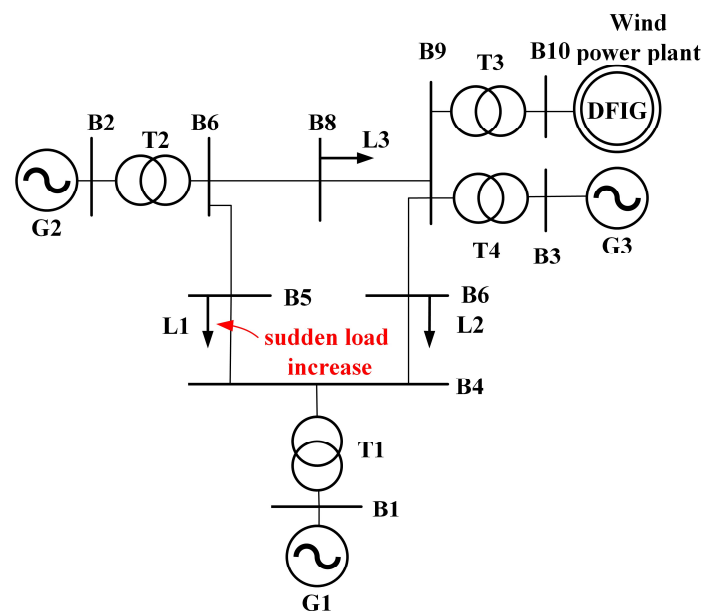
Figure 5. Diagram of the IEEE nine-node system.

The detailed parameters of the simulation system are shown in Appendix A. The generators set, lines, and transformer parameters adopt the Simulink's own parameters. DFIGs and the other parameters are set according to reference [29].

According to the detailed parameters in Appendix A, we can calculate the frequency domain parameters of the SFR model based on the calculation methods in [18]. The frequency domain response parameters are shown in Table 1.

Table 1. The frequency-domain response parameters in small-scale system.

Parameter Name	Parameter Value
D	2
T	12 s
a	0.0812
M	12 s
R	0.0124

　　　DFIG wind farm and synchronous generator set G3 are, respectively, connected to bus 9 through a transformer. The wind farm is composed of DFIG with a rated capacity of 1.5 MW, and the wind speed is 9 m/s. The new energy permeability of the power grid is changed by changing the number of wind farm units and the load level of each node. The sudden load increase fault is set at the load L_1 according to different simulation requirements.

　　　In order to verify the effectiveness of the proposed model and the accuracy of the calculation formula, two different cases based on the small system are set for simulation verification, as shown below:

　　　Case 1: equal proportion of power disturbance occurs under different permeability conditions of wind power. Compare the frequency response in the frequency-domain and time-domain to verify the accuracy of the model.

　　　Case 2: equal proportion of power disturbance occurs under the same permeability of wind power. Compare the frequency response under different control parameters to verify the effectiveness of the proposed calculation method of control parameters.

4.1.2. 39-Bus System

　　　The IEEE three-machine nine-node system is too small to reflect the frequency response of the real system. This paper models the IEEE-bus New England test system by DIgSILENT Power Factory. The system structure topology is shown as Figure 6. Replace the two synchronous units G30 and G37 with wind farms and modify the permeability of the wind power by changing the output of DFIGs unit. The detailed parameters of the AVRs and turbine governors are set according to reference [28]. The frequency domain response parameters are shown in Table 2, according to [18,28]. The wind farm parameter setting is the same as the Section 4.1.1. The sudden load increase fault is set on Bus 26.
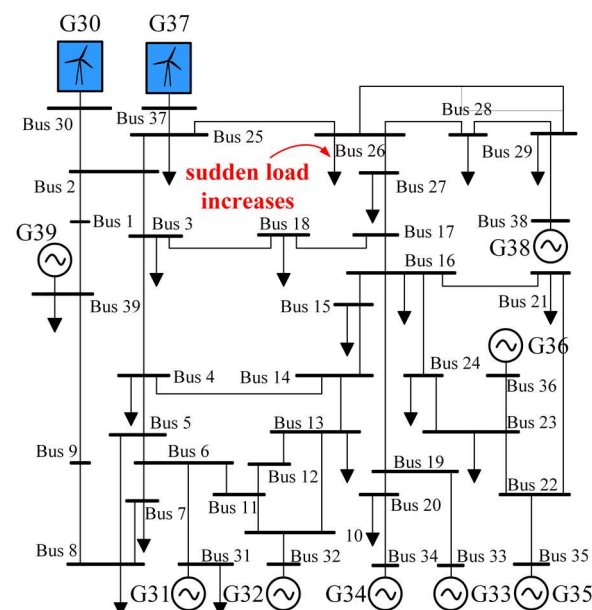
Figure 6. Diagram of the 39-node system.

Table 2. The frequency-domain response parameters in IEEE 39-node system.

Parameter Name	Parameter Value
D	0.3
T	8 s
a	0.3
M	4 s
R	0.05

Based on the 39-node system, this paper sets the Case 3:

The permeability of wind power is 20%, and all the DFIGs will participate the frequency response. The case 3 sets the system load in Bus 26 to generate 5% power step disturbance at 10 s. At the same time, this case sets the frequency modulation parameters of the DFIG, according to the calculations in Section 3. Compare the frequency response in the frequency-domain and time-domain to verify the accuracy of the model in large scale system.

4.2. Case 1 Simulation Analysis

In order to verify the correctness of the model proposed this paper, it will be divided into two scenarios: DFIG participating in frequency modulation and not participating in frequency modulation for time-domain and frequency-domain simulation. Compare the reasonable degree of frequency variation between time-domain simulation and frequency domain simulation system, including the frequency response model of the traditional power system (from now on referred to as model 1) and the frequency response model of wind power highly penetrated system (from now on referred to as model 2).

4.2.1. Scenario 1

Scenario 1 sets the wind power permeability to 20%, and the wind power does not participate in the frequency response, that is, $A_1 = A_2 = 0$, and sets the system load L_1 to generate 6% power step disturbance at 10 s.

As shown in Figure 7, when the DFIG does not participate in the system frequency response, the DFIG output active power remains stable, the rotor speed deviation is tiny, only 0.002 pu, and the rotor speed curves in frequency-domain and time-domain fit well. Comparing the frequency-domain response curves of model 1 and model 2 in Figure 8, the error data can be obtained, as shown in Table 3. The system frequency response curve considering the rotor speed offset proposed in model 2 can better fit the actual system frequency change.
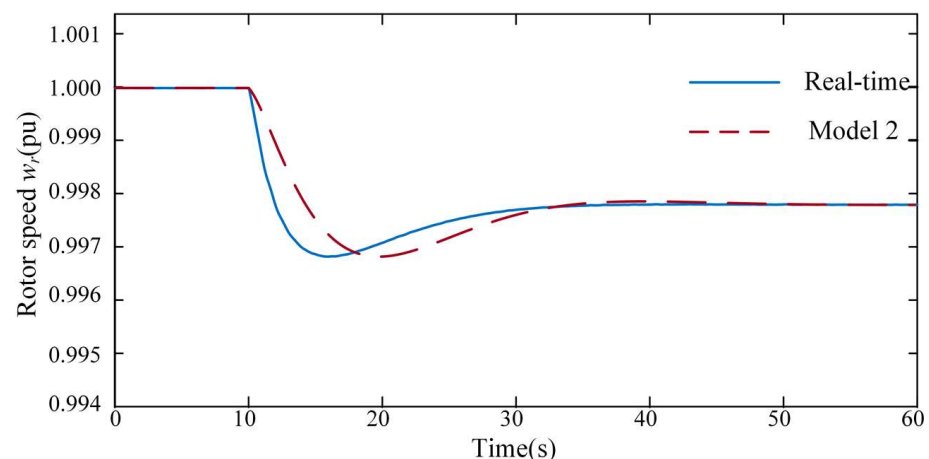
Figure 7. Simulation results of DFIG root speed in scenario 1.
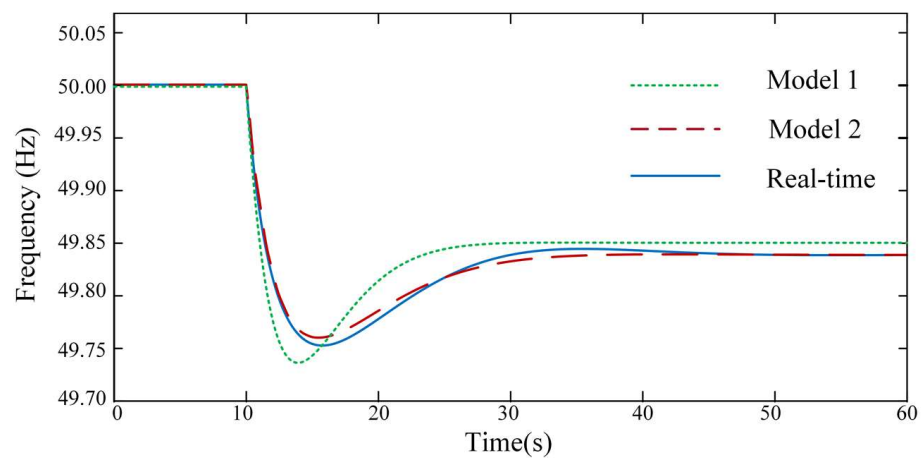
Figure 8. Simulation results of system frequency in scenario 1.

Table 3. Frequency error calculation in small scale system.

		Frequency Lowest Point Error	Steady-State Frequency Error
Scenario 1	Model 1	0.03 Hz	0.02 Hz
	Model 2	0.01 Hz	0
Scenario 2	Model 1	0.05 Hz	0.07 Hz
	Model 2	0.01 Hz	0

4.2.2. Scenario 2

Scenario 2 sets the wind power penetration rate to 30%, and the DFIG participates in the frequency response, and sets the system load L_1 to generate 10% power step disturbance at 10 s.

As shown in Figure 9, when the DFIG participates in the system frequency response, the DFIG rotor speed decreases for power support to 0.8 pu and the rotor speed curves in the frequency-domain and time-domain fit well. Comparing the frequency responses of different models in Figure 10, combined with Table 3, it is proved that model 2 can better fit the actual frequency change of the system at the lowest point of the system frequency and the steady-state frequency point of the system than model 1.
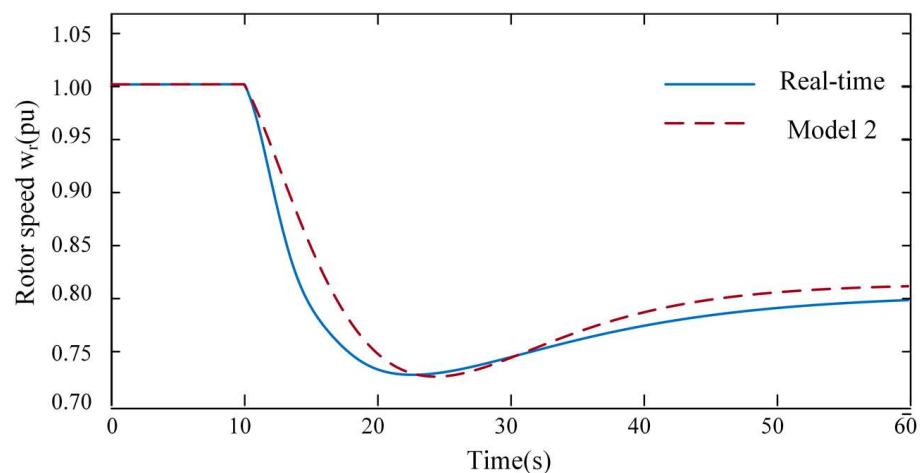
Figure 9. Simulation results of DFIG root speed in scenario 2.
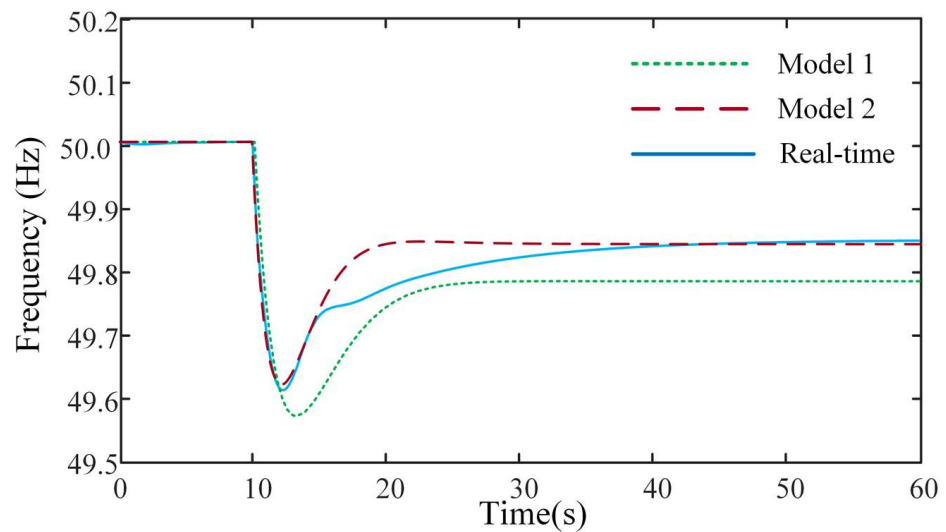
Figure 10. Simulation results of system frequency in scenario 2.

Combined with the simulation results of the two scenarios, when the system does not participate in the frequency response, the error between model 1 and the actual frequency response is small. However, when the system engages in the frequency response, the error increases obviously, so it can no longer fit the exact frequency response. At the same time, it can be verified that when DFIG participates in or does not participate in frequency modulation, the error of model 2 is smaller than that of model 1, so it can better fit the actual frequency response curve of the system.

4.3. Case 2 Simulation Analysis

In order to verify the accuracy of the proposed calculation method, Case 2 sets the same wind power permeability, and the DFIG participates in the frequency response through different control strategy parameter combinations. Set the system load L_1 to generate 10% power step disturbance at 10 s.

Concerning the action threshold of relay protection, this section sets the maximum allowable dynamic frequency change rate of the system as $\eta_1 = \pm0.5$ Hz/s. With reference to the low-frequency load shedding action conditions, this section sets the maximum acceptable dynamic frequency deviation of the system as $\eta_2 = 0.5$ Hz. The maximum permissible frequency deviation of the power system is $\eta_3 = \pm0.2$ Hz.

In Figure 11, 7 groups of different frequency response control combinations are set, but only five of them can be observed, which is in line with the analysis of the steady-state frequency deviation of the system in Section 3.

According to the calculation in Section 3.4, the system meets the requirements of steady-state frequency deviation is $A_1 > 0$. In all control mode combinations, the system's steady-state frequency deviation requirements are met, which verifies the previous theoretical calculation.

Calculate the RoCoF according to the frequency response of the seven different control parameter combinations set, as shown in Figure 12. According to the calculation formula (20) proposed in Section 3.2, when $A_2 > 2.13$, the system meets the maximum frequency change rate requirements. However, as shown in Figure 12, when $A_2 > 2.5$, the maximum frequency change rate of the system meets the requirements; when $A_2 < 1.5$, the maximum frequency change rate of the system is greater than 0.5 Hz/s. It shows that the calculation formula proposed in Section 3.2 has errors within the allowable range and verifies the correctness of the theoretical calculation.
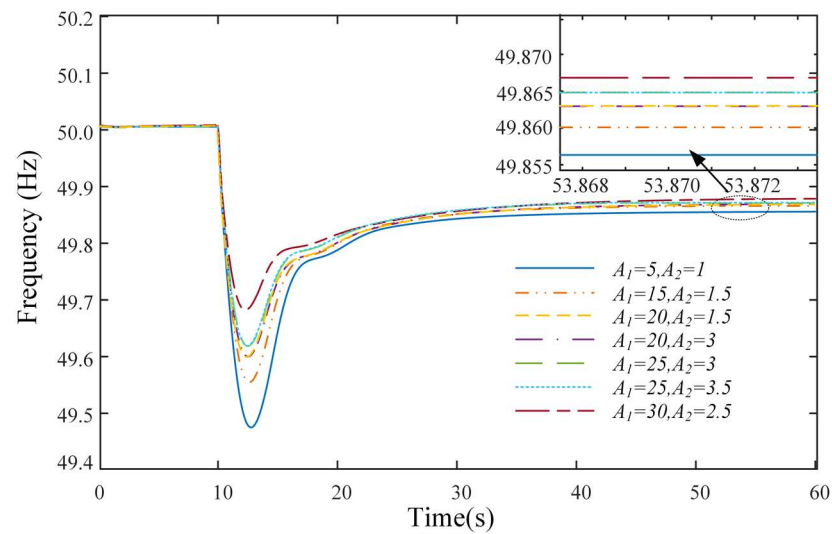
Figure 11. The results of scenario 2 system frequency simulation.
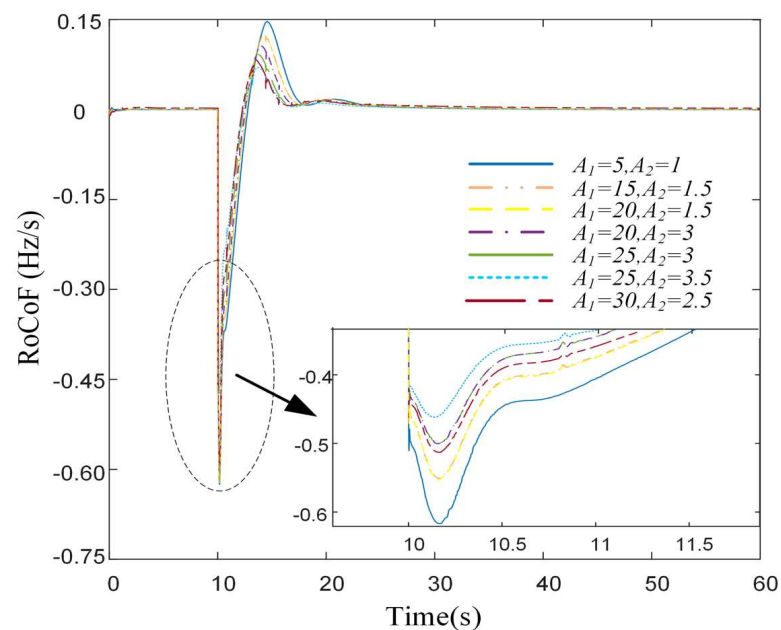
Figure 12. The results of the RoCoF simulation.

4.4. Case 3 Simulation Analysis

The system contains multiple generators sets and they are dispersed. When power disturbance occurs in the system, the frequency maybe different on different busbars. In order to simplify the analysis, the authors select the frequency on bus 26, which is close to the sudden load increase. The IEEE-bus New England test system is typical 60 Hz system. In order to compare the change of system frequency more directly, the unit value is used for plotting as Figure 13 shows.

When the power disturbance occurs at 10 s, the frequency decreases immediately. The lowest point of the system frequency reaches 49.6. The comparison of frequency response errors of the two models is shown in Table 4. Whether the frequency lowest point or the steady-state frequency, the model proposed this paper can better fit the frequency response of actual system.
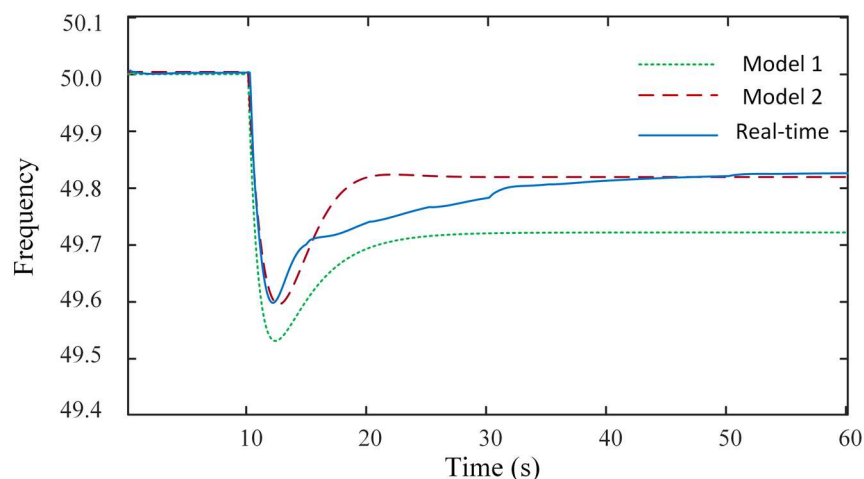
Figure 13. The results of case 3 system frequency simulation.

Table 4. Frequency error calculation in large scale system.

		Frequency Lowest Point Error	Steady-State Frequency Error
Case 3	Model 1	0.04 Hz	0.05 Hz
	Model 2	0.01 Hz	0

5. Conclusions and Research Prospect

5.1. Conclusions

The paper proposes the frequency response model of the wind power highly penetrated system based on the existing researches. It can not only fit the existing system frequency response better than TSFR, but also reflect the working state of DFIG. Based on this model, it calculates quantitatively the specific values of DFIG frequency modulation parameters, considering the power system's stable requirement. The validity of the model and the accuracy of the proposed formula is verified by the time-domain simulation of small-scale and large-scale systems.

5.2. Research Prospects

The frequency response model proposed in this paper equates all DFIG in the system to one, which cannot reflect the working state of a single wind turbine. In practice, the working state of the fan is different, and the response ability of participating frequency is different. It only considers two relatively simple frequency response control strategies. When other frequency response control strategies are considered, the calculation will become very complex and there will be the possibility of non-closed loop.

Therefore, the research prospects are as follows:

- Establishing DFIG frequency response models under different working states (the focus of the next work).
- Simplifying the calculation of the system frequency stable indexes when the SFR model considers the complex frequency response control strategies.

Appendix A

Table A1. IEEE's three-machine nine-node parameters (from Matlab/Simulink).

Classification	Parameters	Values
Synchronous machine (G1, G2, G3)	Nominal power	100 MW
	Line-to-line voltage	13.8 kV
	frequency	50 Hz
	Reactance X_d	1.3125
	Reactance $X_d{}'$	0.1813 pu
	Reactance $X_d{}''$	0.107 pu
	Reactance X_q	1.2578 pu
	Reactance $X_q{}'$	0.4 pu
	Reactance $X_q{}''$	0.107 pu
	Reactance Xl	0.0742 pu
	Inertial time constant H	6.4 s
Transformer (T1, T2, T3)	Nominal power	100 MW
	Frequency	50 Hz
	Winding 1 V1 (Ph-Ph)	13.8 kV
	Winding 1 R1	0.002 pu
	Winding 1 L1	0
	Winding 2 V2 (Ph-Ph)	230 kV
	Winding 2 R2	0.002 pu
	Winding 2 L2	0.0586
	Magnetization resistance	500 pu
	Magnetization resistance	500 pu
Transformer (T4)	Nominal power	100 MW
	Frequency	50 Hz
	Winding 1 V1 (Ph-Ph)	575 V
	Winding 1 R1	0.002 pu
	Winding 1 L1	0
	Winding 2 V2 (Ph-Ph)	230 kV
	Winding 2 R2	0.002 pu
	Winding 2 L2	0.0586
	Magnetization resistance	500 pu
	Magnetization resistance	500 pu
DFIG	Nominal power	1.5/0.9 MW
	Line-to-line voltage	575 V
	frequency	50 Hz
	Stator R_s	0.00706 pu
	Stator L1s	0.171 pu
	Rotor $R_r{}'$	0.005 pu
	Rotor $L1_r{}'$	0.156 pu
	Magnetizing inductance L_m	2.9 pu
	Inertia constant H(s)	5.04 s
	Power at point C	0.73 pu
	Wind speed at point C	12 m/s
	Power regulatorgains[k_p k_i]	[1 100]
	DC bus voltage regulator gains[k_p k_i]	[0.002 0.05]
	Grid-side converter current regulator gains[k_p k_i]	[1 100]
	Rotor-side converter current regulator gains[k_p k_i]	[0.3 8]

References

1. Fernández-Guillamón, A.; Gómez-Lázaro, E.; Muljadi, E.; Molina-García, Á. Power systems with high renewable energy sources: A review of inertia and frequency control strategies over time. *Renew. Sustain. Energy Rev.* **2019**, *115*, 109369. [CrossRef]
2. Olujobi, O.J. The legal sustainability of energy substitution in Nigeria's electric power sector: Renewable energy as alternative. *Prot. Control Mod. Power Syst.* **2020**, *5*, 32. [CrossRef]
3. Tielens, P.; Van Hertem, D. The relevance of inertia in power systems. *Renew. Sustain. Energy Rev.* **2016**, *55*, 999–1009. [CrossRef]
4. Arani, Z.D.; Taher, S.A.; Ghasemi, A.; Shahidehpour, M. Application of Multi-Resonator Notch Frequency Control for Tracking the Frequency in Low Inertia Microgrids Under Distorted Grid Conditions. *IEEE Trans. Smart Grid* **2019**, *10*, 337–349. [CrossRef]
5. Qi, J.; Tang, F.; Xie, J.; Li, X. Effect of DFIG Under Droop Control on Center Migration of Out-of-Step Oscillation. In Proceedings of the 2021 IEEE 5th Conference on Energy Internet and Energy System Integration (EI2), Taiyuan, China, 22–24 October 2021; pp. 2970–2974.
6. Dreidy, M.; Mokhlis, H.; Mekhilef, S. Inertia Response and Frequency Control Techniques for Renewable Energy Sources: A Review. *Renew. Sustain. Energy Rev.* **2017**, *69*, 144–155. [CrossRef]
7. Josephine, R.; Suja, S. Estimating PMSG wind turbines by inertia and droop control schemes with intelligent fuzzy controller in Indian development. *J. Electr. Eng. Technol.* **2014**, *9*, 1196–1201. [CrossRef]
8. Azizipanah-Abarghooee, R.; Malekpour, M.; Dragičević, T.; Blaabjerg, F.; Terzija, V. A Linear Inertial Response Emulation for Variable Speed Wind Turbines. *IEEE Trans. Power Syst.* **2020**, *35*, 1198–1208. [CrossRef]
9. Pepiciello, A.; Vaccaro, A. An Optimization-based Method for Estimating Critical Inertia in Smart Grids. In Proceedings of the 2019 IEEE International Conference on Systems, Man and Cybernetics (SMC), Bari, Italy, 6–9 October 2019; pp. 2237–2241.
10. Sun, M.; Xie, G.; Chen, L.; Liu, Y.; Li, X.; Min, Y. Study on the Necessity and Role of Inertia in Power System Frequency Response. In Proceedings of the 2020 IEEE 4th Conference on Energy Internet and Energy System Integration (EI2), Wuhan, China, 30 October–1 November 2020; pp. 155–159.
11. Wang, S.; Tomsovic, K. Fast Frequency Support from Wind Turbine Generators with Auxiliary Dynamic Demand Control. *IEEE Trans. Power Syst.* **2019**, *34*, 3340–3348. [CrossRef]
12. Jin, C.; Li, W.; Shen, J.; Li, P.; Liu, L.; Wen, K. Active Frequency Response Based on Model Predictive Control for Bulk Power System. *IEEE Trans. Power Syst.* **2019**, *34*, 3002–3013. [CrossRef]
13. Abir, A.; Mehdi, D. Control of permanent-magnet generators applied to variable-speed wind-energy. In Proceedings of the 2017 International Conference on Green Energy & Conversion Systems (GECS), Hammamet, Tunisia, 23–25 March 2017; pp. 1–6.
14. Liu, K.; Qu, Y.; Kim, H.M.; Song, H. Avoiding frequency second dip in power unreserved control during wind power rotational speed recovery. *IEEE Trans. Power Syst.* **2018**, *33*, 3097–3106. [CrossRef]
15. Kayikci, M.; Milanovic, J.V. Dynamic contribution of DFIG-based wind plants to system frequency disturbances. *IEEE Trans. Power Syst.* **2009**, *24*, 859–867. [CrossRef]
16. Wang, S.; Hu, J.; Yuan, X. Virtual synchronous control for grid-connected DFIG-based wind turbines. *IEEE J. Emerg. Sel. Top. Power Electron.* **2015**, *3*, 932–944. [CrossRef]
17. Fazeli, M.; Asher, G.M.; Klumpner, C.; Yao, L.; Bazargan, M. Novel integration of wind generator-energy storage systems within microgrids. *IEEE Trans. Smart Grid* **2012**, *3*, 728–737. [CrossRef]
18. Shi, Q.; Li, F.; Cui, H. Analytical Method to Aggregate Multi-Machine SFR Model with Applications in Power System Dynamic Studies. *IEEE Trans. Power Syst.* **2018**, *33*, 6355–6367. [CrossRef]
19. Li, H.; Wang, J.; Du, Z.; Zhao, F.; Liang, H.; Zhou, B. Frequency control framework of power system with high wind penetration considering demand response and energy storage. *J. Eng.* **2017**, *2017*, 1153–1158. [CrossRef]
20. Wu, Z.; Gao, W.; Gao, T.; Yan, W.; Zhang, H.; Yan, S.; Wang, X. State-of-the-art review on frequency response of wind power plants in power systems. *J. Mod. Power Syst. Clean Energy* **2018**, *6*, 1–16. [CrossRef]
21. Golpîra, H.; Seifi, H.; Messina, A.R.; Haghifam, M. Maximum Penetration Level of Micro-Grids in Large-Scale Power Systems: Frequency Stability Viewpoint. *IEEE Trans. Power Syst.* **2016**, *31*, 5163–5171. [CrossRef]
22. Zhang, J.; Li, M. Analysis of the Frequency Characteristic of the Power Systems Highly Penetrated by New Energy Generation. *Proc. Chin. Soc. Electr. Eng.* **2020**, *9*, 3498–3506.
23. Li, D.; Sun, Y.; Xu, B.; Zhang, J. Minimum inertia and primary frequency capacity assessment for a new energy high permeability power system considering frequency stability. *Power Syst. Prot. Control* **2022**, *3*, 54–61.
24. Garmroodi, M.; Verbic, G.; Hill, D.J. Frequency support from wind turbine generators with a time variable droop characteristic. *IEEE Trans. Sustain. Energy* **2017**, *9*, 676–684. [CrossRef]
25. Ashton, P.; Saunders, C.; Taylor, G.; Carter, A.; Bradley, M. Inertia estimation of the GB power system using synchrophasor measurements. In Proceedings of the 2017 IEEE Power & Energy Society General Meeting, Chicago, IL, USA, 16–20 July 2017; pp. 701–709.
26. Margaris, I.D.; Papathanassiou, S.A.; Hatziargyriou, N.D.; Hansen, A.D.; Sorensen, P. Frequency control in autonomous power systems with high wind power penetration. *IEEE Trans. Sustain. Energy* **2012**, *3*, 189–199. [CrossRef]
27. Kundur, P. *Power System Stability and Control*; McGraw-Hill: New York, NY, USA, 1994; pp. 395–428.

28. Krpan, M.; Kuzle, I. Introducing low-order system frequency response modelling of a future power system with high penetration of wind power plants with frequency support capabilities. *IET Renew. Power Gener.* **2018**, *12*, 1453–1461. [CrossRef]

29. Hu, B.; Tang, F.; Liu, D.; Li, Y.; Wei, X. A Wind-Storage Combined Frequency Regulation Control Strategy Based on Improved Torque Limit Control. *Sustainability* **2021**, *13*, 3765. [CrossRef]